Surface & Coatings Technology 482 (2024) 130695

Contents lists available at ScienceDirect

Surface & Coatings Technology

journal homepage: www.elsevier.com/locate/surfcoat

Transparent low moisture permeable coating for perovskite solar cell encapsulation

Chieh-Ming Tsai [a], Chia-Feng Li [a], Yu-Ching Huang [b], Feng-Yu Tsai [a], Wei-Fang Su [a,b,*]

[a] Department of Materials Science and Engineering, National Taiwan University, Taipei, Taiwan
[b] Department of Materials Engineering, Ming Chi University of Technology, New Taipei, Taiwan

ARTICLE INFO

Keywords:
Moisture permeation
Encapsulation
Transparent
Solventless
Perovskite solar cell

ABSTRACT

The perovskite solar cell has potential to become next generation photovoltaics due to its high power conversion efficiency and easy processing. However, the perovskite solar cell is very sensitive to moisture and temperature which needs to be protected by low temperature processable moisture permeation coating. Furthermore, the encapsulating coating has to be transparent so the perovskite solar cell can be kept its transparency and used in integrated building structure or tandem with Si solar cell, etc. The coating material should be solventless which will not damage the perovskite layer and release any harmful volatile organic compounds during the coating application process. A solventless hybrid coating made from polyfluoroesterimide and silica nanoparticle has been developed which can be cured within minutes using mercury lamp (light intensity 935 W/m^2) at room temperature. The coating exhibits low moisture permeation and high transparency. The performance improvement is due to the presence of water repelling characteristic of fluoro moiety and less moisture permeable inorganic silica component. The encapsulated devices exhibit long-term stability when they were subjected to the environment of 65 °C and 65%RH for >400 h.

1. Introduction

The perovskite solar cell, emerging as a promising next-generation technology of solar energy to electricity, garners attention for its remarkable efficiency and cost-effectiveness in manufacturing [1]. However, unlike silicon-based counterparts, perovskite solar cells are vulnerable to degradation from environmental factors such as humidity, UV-light, and heat [2,3]. Hence, ensuring a dependable encapsulation method for perovskite solar cells becomes crucial for their successful commercialization. The key requisites for an effective encapsulant include a low water vapor permeability (WVP) and high transparency to UV-A and visible light. A low WVP encapsulation significantly mitigates water vapor permeation, thereby prolonging the lifespan of perovskite solar cells [4]. High transparency is essential, especially for transparent solar cells intended for applications like building-integrated structures or tandem solar cells [5]. Additionally, an ideal encapsulant can incorporate light conversion additives capable of absorbing UV light and transforming it into visible light. This feature not only boosts solar cell efficiency but also extends its operational life [6].

Currently, there are four encapsulation methods under consideration: glass-glass encapsulation, polymer encapsulation, thin film encapsulation, and multilayer lamination as shown in Fig. 1 [7]. Glass-glass encapsulation stands as the most prevalent method for perovskite solar cells, entailing the sandwiching of the solar device between two transparent electrode/glass slides using encapsulant adhesive. Various polymer materials have been employed as encapsulants to seal electronic devices, including ethylene vinyl acetate (EVA), copolymers like ethylene and polymethacrylic acid (Surlyn), polyisobutylene (PIB), and UV-curable epoxy resin [8,9]. In this method, the polymeric encapsulant is directly applied onto the perovskite device, followed by the placement of a glass plate atop the polymer to protect the side of perovskite layer from moisture and oxygen exposure. Then, PIB and/or UV-curable epoxy resin is further administered as a thick film along the device's edges to impede moisture/oxygen permeation and enhance the device's lifespan. Encapsulation systems with edge thick film achieve a total water vapor transmission rate lower than 10^{-3} g/m^2·day [10]. For encapsulating flexible devices, polymeric or/and thin film materials can be used. Poly(methylmethacrylate) (PMMA), polyethylene terephthalate (PET), polytetrafluoroethylene (PTFE), and adamamtane (ADA) have been selected as materials for polymeric encapsulation. Conversely, ceramic inorganic materials like Al_2O_3, SiO_X, and TiO_2 are deposited as dense thin films via plasma-enhanced chemical vapor

* Corresponding author at: 1, Roosevelt Rd, Sec. 4, Taipei, Taiwan.
E-mail address: suwf@ntu.edu.tw (W.-F. Su).

https://doi.org/10.1016/j.surfcoat.2024.130695
Received 7 December 2023; Received in revised form 27 February 2024; Accepted 19 March 2024
Available online 20 March 2024

deposition (PECVD) or atomic layer deposition (ALD) [11–13] to seal the device. However, these methods are considered less reliable than the glass-glass encapsulation due to the high moisture permeation of polymers and the fragile nature of nanometer-thin films. To address these limitations, a multilayer system employing alternating layers of polymer and ceramic has been developed to create a robust encapsulation system capable of achieving a total water vapor transmission rate as low as 10^{-6} g/m^2·day [14,15].

Polymers are extensively utilized as encapsulating materials due to their ease of property tuning and processing. An ideal polymeric encapsulant should fulfill several criteria: low water vapor permeation (WVP), high transparency to visible light, robust adhesive strength, mechanical resilience, solvent-free composition, and UV curability. While exceptional transparency is not universally obligatory, it becomes essential for transparent solar cells used in building-integrated structures and tandem solar cell applications. Incorporating down-conversion photoluminescence additives in the encapsulant demands optimal UV-to-visible light transparency to maximize additional light harvesting. Strong adhesive strength is a crucial requirement that prevents the encapsulant from detaching from the substrate and losing its functionality. High mechanical strength is essential to protect the device against external forces during transportation, installation, and exposure to severe weather conditions.

Solventless encapsulants mean the resin materials contain no solvent. Utilizing a solventless encapsulant prevents solvent-related damage to the layers of perovskite and charge transportation in devices, thereby preserving their integrity [16,17]. Additionally, it reduces health hazards associated with solvent evaporation during the encapsulation process. Furthermore, employing a UV-curable encapsulant concludes the encapsulation process within seconds as opposed to minutes required for thermal curing or heat lamination. This not only conserves energy but also eliminates the risk of heat damage to the device.

Polymer, being an organic material, forms an organic/inorganic hybrid when inorganic fillers are incorporated into its matrix [18] This hybridization potentially reduces WVP due to an increased diffusion path for molecules within the hybrid. Dense ceramics act as barriers when water molecules attempt to diffuse towards nearby fillers, compelling the molecules to take detours around these barriers. However, attention must be paid to the interface between the inorganic filler and organic matrix [19]. A relatively poor interface with defects could serve as shortcuts for moisture molecules. Therefore, ensuring good compatibility between filler and matrix becomes imperative [20].

In theory, a filler oriented perpendicularly to the diffusion path—such as a platy filler—provides the most effective barrier effect. However, research examining the relationship between filler shape and WVP discovered that there is no strong effect on filler shape when the fillers are randomly dispersed with the same inorganic content. In cases of random dispersion, achieving high orientation of platy fillers perpendicular to the moisture diffusion direction becomes challenging. Consequently, platy fillers aligned parallel to the diffusion path do not significantly impede moisture movement [21]. Thus, we decide to use spherical SiO_2 nanoparticles, measuring 20–25 nm, as the hybrid resin filler.

Table I lists WVP of common polymers [22]. Polytetrafluoroethylene (PTFE) has the lowest WVP value as low as 0.0045 g·mm/m^2·day when fluorocarbon polymers perform dense and low surface energy surface to repel moisture. On the other hand, other hydrocarbon polymers show at least one order higher WVP than fluorocarbons. Therefore, we synthesize fluorocarbon polymers as the main polymer matrix of the encapsulants, including FEVE-UA, PSFIA and TFEVE-FIDA. They are blended with surface modified silica nanoparticles, acrylate monomers to make solventless UV curable encapsulants. Their properties are evaluated. The results are described and discussed below.

2. Experimental procedure

2.1. Materials

Commercially available polymers were used as received: poly (chlorotrifluoro ethylene-*co*-vinyl ether) (CTFEVE) (AGC, LF-200F), poly(tetrafluoro ethylene-*co*-vinyl ether) (TFEVE)in butyl acetate (65 wt%) (Daikin, GK570). Chemicals for the synthesis of polymers were used as received without further purification except some drying procedures were specified. They are list below: 2-isocyanatoethyl acrylate (IEA) (TCI, 98.0 %), dibutyltin dilaurate (DBTDL) (TCI, 95.0 %), ethyl acetate (Fisher, 99.5 %), 4,4′-(hexafluoroisopropylidene) diphthalic anhydride (6FDA) (Fluorochem, 98.0 %), 4,4′-

Table I
Water vapor permeability of common polymers.

Material	WVP (g•mm/m^2•day)
Polystyrene (PS)	0.8–3.9
Acrylonitrile Butadiene Styrene (ABS)	2.0–6.3
Polyamides (PA)	0.24–125
Mid Density Polyethylene (MDPE)	0.4–0.6
Polytetrafluoroethylene (PTFE)	0.0045–0.3
Fluorinated ethylene propylene (FEP)	0.087
Polymethyl Methacrylate (PMMA)	1.7

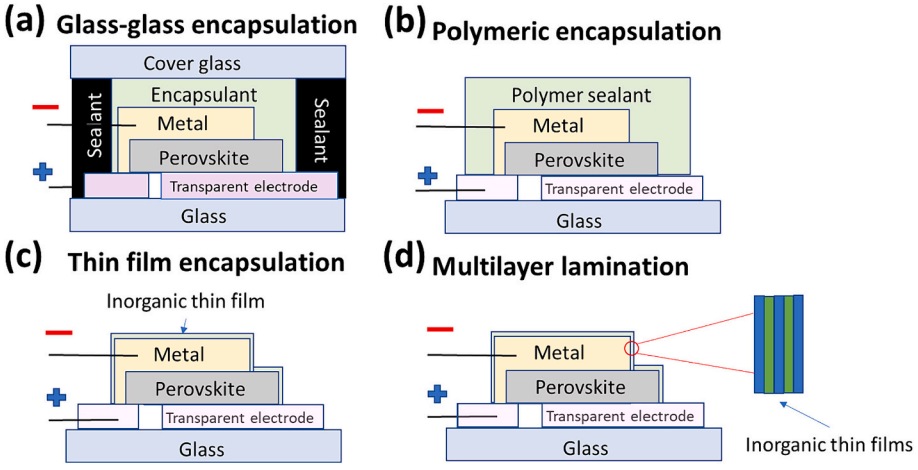

Fig. 1. Four possible encapsulation systems for perovskite solar cell (a) glass-glass encapsulation (b) polymeric encapsulation (c) thin film encapsulation and (d) multilayer lamination.

(hexafluoroisopropylidene) dianiline (6FpDA) (ACROS, 98.0 %), acetic anhydride (ACROS, 99.0 %), pyridine (Fisher, 99.0 %), *N*,*N*-dimethylacetamide (DMAc) (ACROS, 99.5 %), 2-hydroxyethyl methacrylate (HEMA) (ACROS,97.0 %), 1,6-hexanediol diacrylate (HDDA) (TCI, 98.0 %), neopentyl glycol diacrylate (NPGDA) (TCI, 89.0 %), tricyclodecane dimethanol diacrylate (TCDDA) (Shin-Nakamura, NK Ester DCP), 2-phenoxyethyl acrylate (PEA) (TCI, 93.0 %), 1H,1H,7H-dodecafluoroheptyl acrylate (12FHA) (TCI, 97.0 %), 3-(trimethoxysilyl)propyl methacrylate (MPS) (ACROS, 98.0 %), (heptadecafluoro-1,1,2,2-tetrahydrodecyl) triethoxysilane (HFTES) (Gelest, 97.0 %), methanol (Fisher, 99.8 %), photoinitiator IRGACURE^{R} 184:1-hydroxy-cyclohexyl-phenyl-ketone (Irg 184, Ciba). Nano silica (~25 nm) dispersed in methanol (40 wt% solid, Nissan, MA-ST-M) was used as filler. Commercial encapsulant: A901452-TXS (ACW Co.) used as a control to evaluate the effectiveness of developed encapsulant for perovskite solar cell.

2.2. Synthesis of UV curable polymer FEVE-UA

TFEVE polymer solution of 1.54 g was dried in a flask at 90 °C for 2 h to obtain a solid form. CTFEVE flake or TFEVE of 1 g and 5 ml ethyl acetate were placed in a reaction flask under stirring overnight to make a well dissolved solution mixture. DBTDL of 6 μl and appropriate amount of IEA (0.16 g for TFEVE and 0.123 g for CTFEVE) were added into the solution mixture and mixed further for 30 min under stirring. Then the reaction mixture was reacted at 75 °C for 24 h in N_2 under stirring. After cooling down, the product was transferred to a sample vial for storage and characterization.

2.3. Synthesis of UV curable polymer PSFIA

6FDA of 4.09 g was dissolved in 23 ml DMAc in a three neck round bottom flask. Separately, 6FpDA of 1.5 g was also dissolved in 11 ml of DMAc in a 20 ml sample vial. Then the 6FpDA solution was slowly injected into the flask at 5 ml/h via a syringe pump to react it with the 6FDA solution under stirring in N_2. After 24 h reaction at room temperature, the reaction flask was placed into a 90 °C oil bath, a mixture of 1.84 g acetic anhydride and 1.79 g pyridine as catalyst was injected into the reaction flask. After reacting overnight, the light-yellow solution was dropped into 300 ml of DI water and centrifuged at 10000 rpm for 7 min. The white precipitate product was obtained by decanting the liquid. The product was dried at 160 °C in a vacuum tubular furnace for 24 h. The product was named FIDA.

To get PSFIA, 4 g FIDA was dissolved in 24 ml DMAc in a 100 ml 3 neck round bottom flask. The flask was covered with Al-foil to protect acrylate product curing by the room light. HEMA of 2.2 g (stored in Drierite) was dried using dry air purging for 1 h. The dried HEMA and 0.029 g of hydroquinone were added into the reaction flask and reacted with FIDA/DMAc solution under stirring at 75 °C for 24 h in dry air. The reaction product was poured into one liter of DI water to form white precipitate product. The product was collected by filtration and was dried at 120 °C for 48 h in a vacuum tubular furnace. The product was named PSFIA.

2.4. Synthesis of TFEVE-FIDA polymer solution

TFEVE polymer solution of 2.08 g was placed in a three neck round bottom flask and heated at 90 °C for 2 h to remove butyl acetate. Then TFEVE was dissolved into 12 ml ethyl acetate overnight under stirring. FIDA of 1.6 g was dissolved in 10 ml, then injected into the flask containing TFEVE. The mixture was reacted at 75 °C for 48 h under stirring in N_2 to obtain reaction product. The product solution was stored in a 50 ml glass vial.

2.5. Surface modification of SiO_2 nanoparticles

Nissan SiO_2 methanol dispersion of 12.5 g was diluted with 20 ml methanol in a three neck round bottom flask equipped with reflux condenser. Appropriate amount of MPS or HFTFS was added into the reaction flask. The reaction mixture was reacted at 50 °C for 24 h with stirring under refluxing. The chemical formulations of silane-modified SiO_2 reaction are listed in Table S1. The characterization of modified SiO_2 nanoparticle is described in Supporting Information.

2.6. Preparation of solventless organic resins

To make solventless resins, appropriate amount of FEVE-UA, PSFIA or TFEVE-FIDA solution was mixed with different diacrylate monomers at different concentration according to the formulations listed in Tables S2, S3 and S4. Photoinitiator Irg 184 of 4 wt% was added into the resin basis on the weight of resin. The solvent of TFEVE-FIDA based organic resin was removed by vacuum at room temperature. The resins were stored in Al-foil covered sample vial.

2.7. Preparation of solventless hybrid resin

Appropriate amount of FEVE-UA, PSFIA or TFEVE-FIDA and SiO_2 filler were mixed with different type and amount of diacrylate monomers to form different formulations as shown in Tables S5, S6 and S7. Photoinitiator Irg 184 of 4 wt% was added into the resin basis on the weight of neat resin. The majority of solvents of hybrid resin was removed by drying the mixture in air for two days and then further treated with vacuum to remove residue solvent. The hybrid resins were stored in Al-foil covered sample vials.

2.8. Preparation of films of encapsulants

The films of encapsulating resins were prepared by casting method. Fig. S1 shows the schematic diagram of encapsulating film preparation. For a free-standing film sample, a wet resin was filled in a hollow mold (5 cm in diameter and 100 μm in thickness, made by 3D printing) resting on a PET film, then another PET film was placed on top of the mold. A glass rod was placed on the top layer of PET, drawn down slowly from top to bottom of PET layer, and to squeeze out any excess resin. Then the sample was cured by a high-powered UV-lamp box (OPAS, Xlite 400Q) for 2 min. The free-standing film about 100 μm thickness was obtained by removing top layer PET. For adhered film on substrate, two 50 μm thick tape spacers were pasted with a distance of 1.5 cm in between on the glass or quartz substrate. A drop of resin was placed on the substrate between the spacers, then covered the resin with PET. A glass rod was placed on the top layer of PET, drawn down slowly from top to bottom of PET layer, and to squeeze out any excess resin. Then the sample was cured by a high-powered UV-lamp box (OPAS, Xlite 400Q) for 2 min. By removing the top PET, the adhered film of about 50 μm on substrate was obtained. The film on quartz substrate was used to measure its transparency using UV–vis analysis.

2.9. Water vapor transmission rate analysis of encapsulating films

The WVTR of films were measured according to ASTM E96 method. The setup was shown in the Fig. S2. Water was added into a permeability cup, then the 10 cm^2 sample was mounted on the cup and tight up by the fringes for moisture permeation measurement. The samples were placed in a desiccator containing Drierite which can control the humidity below 5%RH at 23 °C. The humidity and temperature were recorded by the thermometer/humidity meter placed in the desiccator. The water weight loss of each day was measured for 7 days, then the WVTR and WVP of samples can be calculated according to the following equations.

$$\mathrm{WVP} = \frac{m \cdot d}{A \cdot t}.$$

where m is the mass of the vapor, d is the thickness of encapsulant, t is

the duration of exposure to moisture and A is the surface area which exposed to moisture.

2.10. Transparency of encapsulating films

The transparency of samples was measured by UV–vis spectroscopy (JASCO, V-650) from 250 to 800 nm. After taking a blank quartz as background, the transmittance of the 50 μm thick samples on the quartz can be measured.

2.11. Preparation of encapsulated devices for accelerated aging test

In order to evaluate the effectiveness of the neat encapsulating coating, the black sealant as shown in Fig. 1(a) was not used in the device encapsulation for this research. The encapsulating procedure was carried out in the nitrogen filled glove box. The neat encapsulating resin was applied one drop on the cover glass using 1 cm^3 syringe. Then the resin loaded glass plate was place on top of device to form a thin coating about 50 μm. The glass was held in place by the adhesive strength of neat encapsulating resin.

3. Results and discussion

3.1. FEVE-UA based encapsulating coating

Fig. 2 presents the synthetic diagram detailing the structure of the FEVE-UA polymer, where IEA is grafted onto the aliphatic FEVE through urethane bonding. Characterization of the FEVE-UA polymer is based on FT-IR analysis, with its spectrum shown in Fig. S3. The detailed explanations of FTIR spectrum are in the supporting information. The results confirm the successful synthesis of FEVE-UA polymer.

Assessing the performance of the encapsulating coating, Table II lists the WVP results of the FEVE-UA-based coating. Notably, all WVP values for the FEVE-UA encapsulating films are below 2.3 g·mm/m^2·day, with the lowest reaching 1.59 g·mm/m^2·day. This low value is attributed to the aliphatic fluoropolymer's high fluorine atom content, which contributes to low surface energy and a densely packed linear structure. However, an observed yellow hue in the resin interacting with perovskite suggests a reaction, likely stemming from unreacted isocyanato ethyl acrylate (IEA) or hydroxyl groups on the FEVE. To prevent these groups from adversely affecting the perovskite, additional reactions or treatments during the preparation of the FEVE-UA polymer are necessary. This step aims to mitigate such interactions, preventing discoloration of the perovskite material upon contact with the composite resin. Therefore, we developed another fluoropolymer system with aromatic imide chain which expected more mechanical and thermal robust than this aliphatic urethane system containing less stable urethane linkage [23].

Table II
WVP of FEVE-UA based polymeric encapsulating films.

Sample	WVP (g•mm/m^2•day)
P-resin1	1.95
P-resin2	1.84
P-resin3	2.28
P-resin4	1.59
P-resin5	2.06

3.2. PSFIA based encapsulating coating

Fig. 3 depicts the synthetic diagram outlining the structure of the aromatic PSFIA polymer. The precursor, FIDA, is initially synthesized and then undergoes a reaction with HEMA, resulting in the formation of acrylic functional groups for crosslinking and carboxyl functional groups to facilitate strong adhesion to glass surfaces. Both FIDA and PSFIA undergo characterization through NMR and FT-IR analyses, with their respective spectra presented in Figs. S4 to S6. The detailed explanations of FTIR spectrum are in the supporting information. The results confirm the successful synthesis of PSFIA polymer.

Table III provides the WVP values of the polymeric encapsulating films based on PSFIA. These values range between 2.0 and 3.4. Notably, the sample labeled P-resin11, with a WVP of 2.07 g·mm/m^2·day, exhibits a relatively higher fluorine atom content, suggesting the potential for further WVP reduction. Conversely, the sample lacking additional functional acrylate monomers, such as P-resin6, shows a comparatively higher WVP of 3.38 g·mm/m^2·day. Fig. 4 displays the UV–vis spectra of the PSFIA-based polymeric encapsulating films. All polymeric samples maintain over 90 % transmittance in the visible light range of 400-800 nm, indicating excellent compatibility between polymers and dilutant monomers. This compatibility effectively prevents substantial phase separation on a larger scale.

Table IV outlines the WVP of hybrid encapsulating films based on PSFIA. Comparing these with the polymeric samples, the WVP values vary further due to differing compatibilities between the polymer matrix and filler materials. Among the hybrid samples, H-resin9–3 demonstrates the lowest WVP of 1.87 g·mm/m^2·day, attributed to HDDA's superior dense packing compared to NPGDA, thus enhancing moisture resistance. However, despite this advantage, the organic matrix exhibits poor compatibility with inorganic SiO_2, leading to particle aggregation and light scattering observed in the UV–vis measurement, as illustrated in Fig. 5. Conversely, while maintaining over 90 % visible light transmittance, certain samples fail to achieve low WVP due to heterogeneous defect interfaces between organic matrix and inorganic filler.

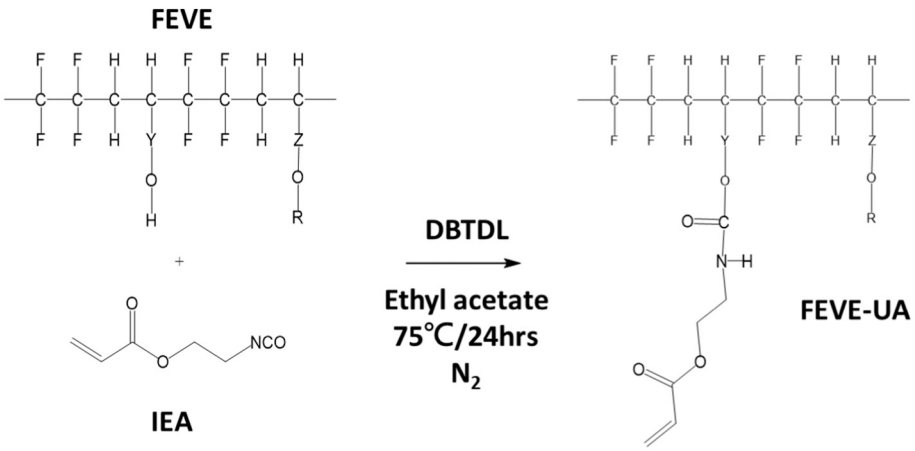

Fig. 2. Synthetic diagram of FEVE-UA polymer.

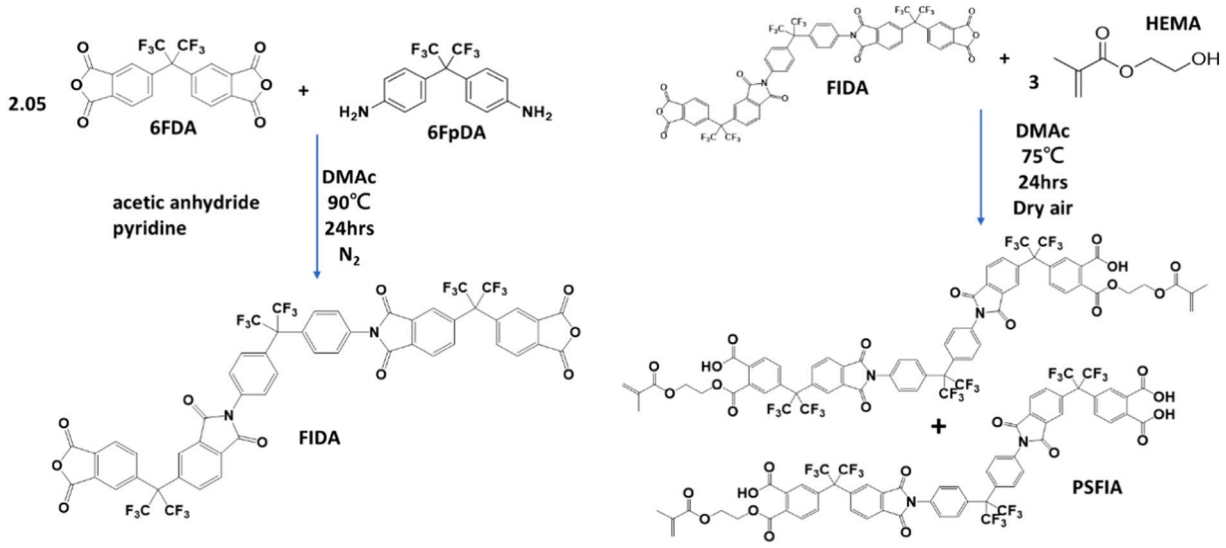

Fig. 3. Synthetic diagram of PSFIA polymer.

Table III
WVP of PSFIA based polymeric encapsulating films.

Sample	WVP (g•mm/m^2•day)
P-resin6	3.38
P-resin7	2.17
P-resin8	2.11
P-resin9	2.78
P-resin10	2.49
P-resin11	2.07
P-resin12	2.17
P-resin13	2.06
P-resin14	3.43
P-resin15	3.17

Table IV
WVP of PSFIA based hybrid encapsulating films.

Sample	WVP (g•mm/m^2•day)
H-resin5-1	3.60
H-resin5-2	3.52
H-resin5-3	3.63
H-resin6-3	2.28
H-resin7-3	3.07
H-resin8-3	1.87
H-resin9-1	2.91
H-resin9-2	2.25
H-resin9-3	2.72
H-resin10-3	3.40
H-resin11-3	2.78
H-resin12-3	3.42
H-resin13-1	2.67

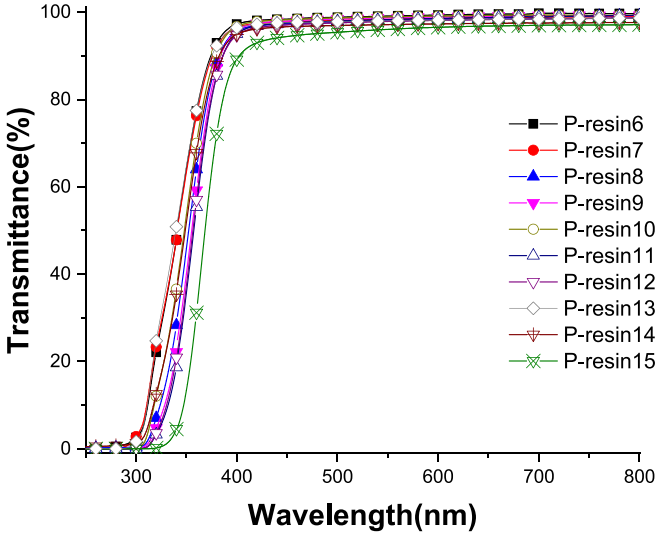

Fig. 4. UV–vis spectra of PSFIA based polymeric encapsulating film (50 μm).

3.3. TFEVE-FIDA based encapsulating coating

Fig. 6 illustrates the synthetic diagram detailing the TFEVE-FIDA polymer, formed through the combination of aliphatic TFEVE and aromatic FIDA. This unique combination maintains the low WVP characteristic of FEVE polymer while avoiding highly reactive isocyanate functional groups. The presence of aromatic FIDA not only ensures good thermal stability and adhesion to glass but also contributes to a high fluorine atom content. The TFEVE-FIDA polymer is characterized by the FTIR (Fig. S7). The detailed explanations of FTIR spectrum are presented in the supporting information. The results confirm the successful synthesis of the polymer.

Table V presents the WVP values of the TFEVE-FIDA-based encapsulating coating. Notably, H-resin14-1 and H-resin15-2 exhibit low WVP values of 2.09 and 1.67 g·mm/m^2·day, respectively. Additionally, Fig. 7 showcases the high transmittance of both samples in the visible light region. The TFEVE-FIDA-based hybrid samples achieve WVP values below 2.1 g·mm/m^2·day and maintain over 90 % transmittance in the visible light region simultaneously.

3.4. Performance of encapsulating coating

H-resin14-1 was specifically chosen as the encapsulating film for the perovskite solar cell due to its exceptional properties: it boasts high transmittance in both visible light (over 96 %) and UV spectrum (90.1 % at 360 nm), alongside a remarkably low WVP of 2.09 g·mm/m^2·day. Fig. 8 compares H-resin14-1 with the control. In Fig. 8(a), the superior transmittance of H-resin14-1 is clearly depicted, showcasing its higher transparency compared to the control. Moreover, Fig. 8(b) highlights the similarity in WVP values between the H-resin14-1 sample and the control.

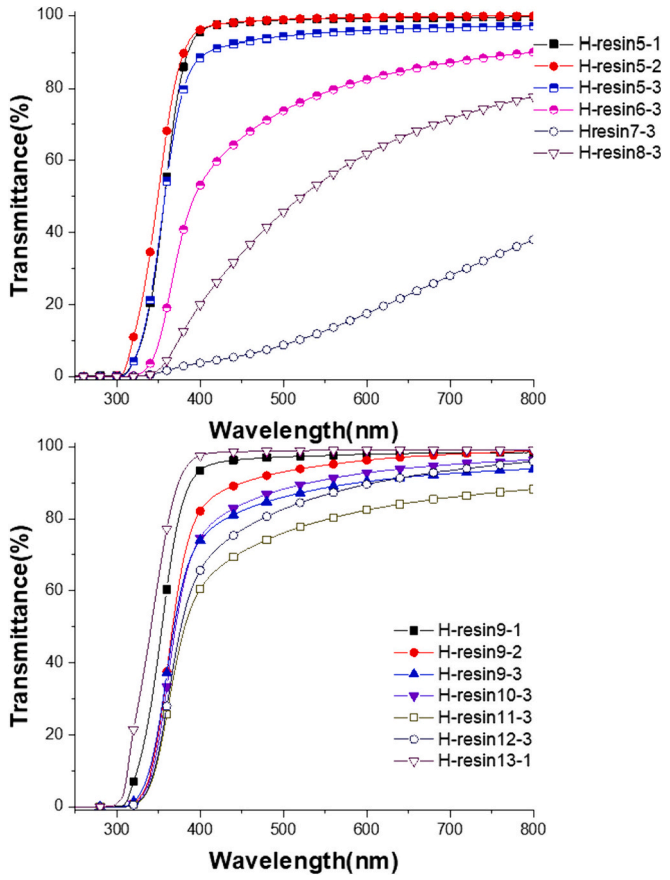

Fig. 5. UV–vis spectra of PSFIA based hybrid encapsulating film (50 μm).

3.5. *Performance of perovskite solar cell with encapsulation without aging and with aging test*

The details of device fabrications and measurements are shown in supporting information. Effects of encapsulation on the performance of solar cells are shown in Fig. S11 without aging. Fig. S11(a) presents the J-V curves and Fig. S11(b) shows the EQE results of encapsulated perovskite solar cells. The curves show resemblance results. The similar EQE curves indicate the band structure alignment of the devices shows no differences after encapsulation. The similar results of Voc, Jsc, FF and PCE mean the performance of devices don't change by the encapsulation. Fig. S11(c) summaries the performances of solar cells. As a result, control resin and H-resin14-1 don't react or affect each layer of devices after direct contact to the devices and UV-curing.

Fig. 8(c) concludes the results of accelerated lifetime test for encapsulated perovskite solar cells. In order to evaluated the effectiveness of the neat encapsulating coating, the black edge sealant as shown in Fig. 1(a) was not used in the device encapsulation for this research. Following exposure to conditions of 65 °C and 65%RH for 400 h, the solar cells encapsulated with H-resin14-1 exhibit an impressive outcome. The PCE remains over 85 % of its original value, highlighting the remarkable protective capabilities of H-resin14-1 from heat and moisture and better than the control of 80 % of its original PCE. The changes of PCE, Voc, Jsc, and FF and their normalized data upon

Table V
WVP of TFEVE-FIDA based polymeric and hybrid encapsulating films.

Sample	WVP (g•mm/m^2•day)
P-resin16 (polymer)	1.67
P-resin17 (polymer)	2.08
H-resin14-1 (hybrid)	2.09
H-resin15-2 (hybrid)	1.67

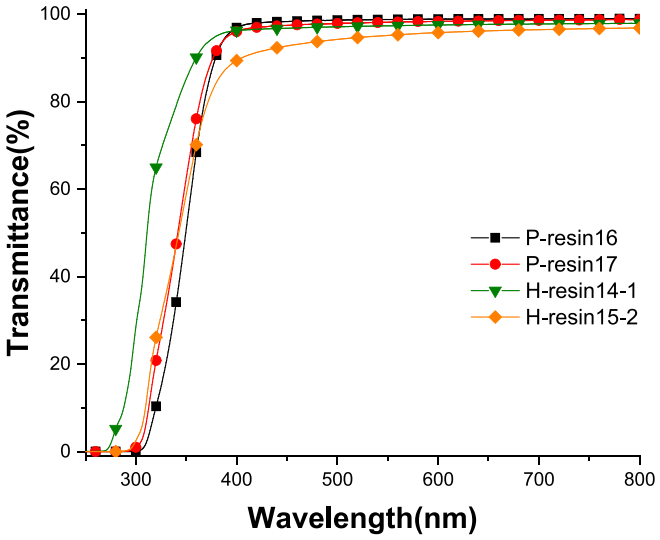

Fig. 7. UV–vis spectra of TFEVE-FIDA based polymeric and hybrid encapsulation film (50 μm).

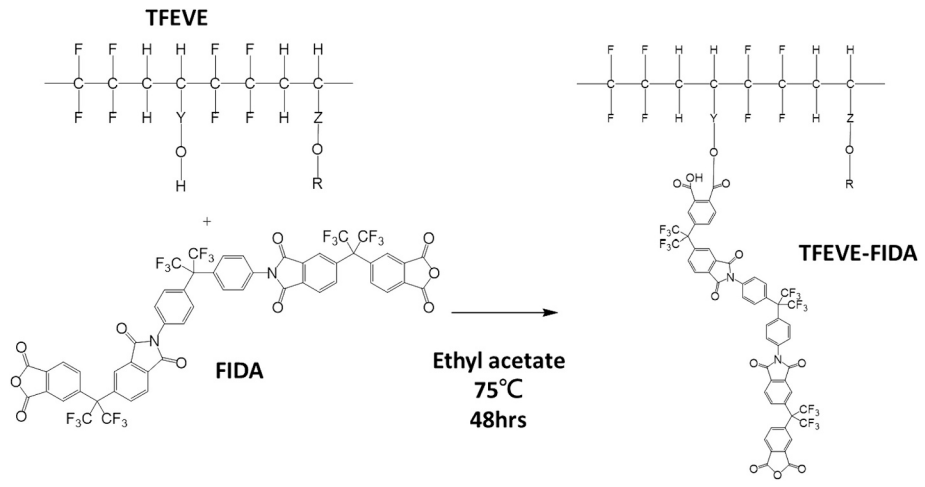

Fig. 6. Synthetic diagram of TFEVE-FIDA polymer.

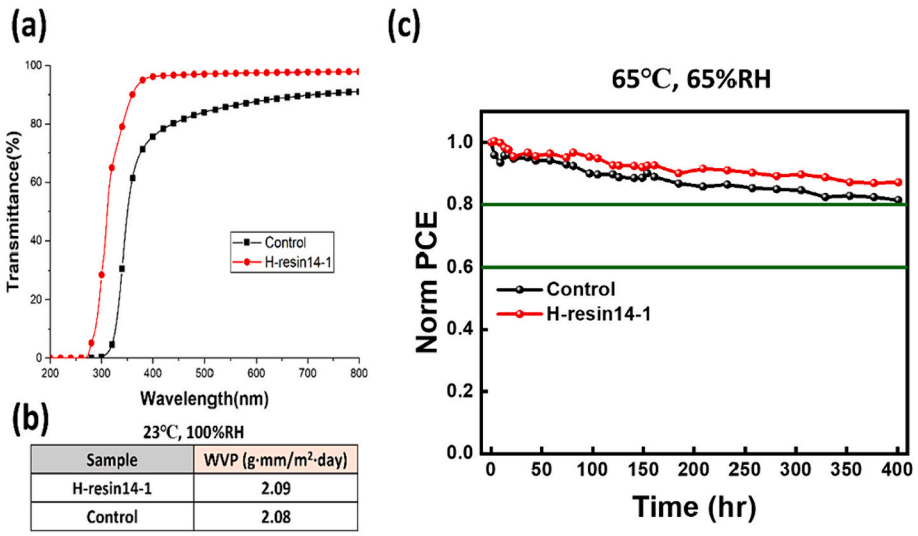

Sample	WVP (g·mm/m²·day)
H-resin14-1	2.09
Control	2.08

Fig. 8. (a) UV–vis spectra and (b) WVP data of thin films of H-resin14-1 and control, (c) accelerated life time test results of encapsulated perovskite solar cells under 65 °C and 65%RH.

accelerated lifetime experiments are shown in Figs. S12 and S13 respectively. The devices were encapsulated in the nitrogen glove box thus the oxygen effect on the life of device was not considered [[24]]. The moisture decreases the PCE of devices, shows almost no effect to the Voc, slightly decrease to Jsc and relatively large effect to FF. The main reason decreases the PCE of devices is from the decaying perovskite absorbing layer, thus less photocurrent is being generated. The encapsulant is inert organic-inorganic materials which acts as protective layer and does not react with perovskite layer, charge transport layers and electrodes in the accelerated life test [1]. Fig. S14 shows the devices retain their integrity after 200 h aging test at 65 °C and 65%RH. Our goal has been achieved to have encapsulants that possess commendable WVP, optical transparency and long-term protecting devices as shown in the rigorous 65 °C, 65%RH accelerated lifetime test.

4. Conclusion

In this research, three different polymers were developed and used in the encapsulating resin for perovskite solar cell. Aliphatic FEVE-UA based polymeric encapsulating coating shows good WVP but it reacts with perovskite. Aromatic thermal stabled PSFIA based encapsulating coatings cannot meet the requirements of low WVP (2.2 g•mm/m^2•day) and high transparency (>90 % transmittance in visible range) in the same time. The combination of aliphatic TFEVE and aromatic imide FIDA forms TFEVE-FIDA polymer. Incorporating SiO_2 nanoparticles in this polymer, TFEVE-FIDA hybrid resins are generated. They perform low WVP and high transmittance of UV and visible light because the high content of fluoro moiety in the resin and high compatibility between the resin and SiO_2 nanoparticles. The TFEVE-FIDA hybrid coating can protect the perovskite solar cell in 65 °C, 65RH% condition for over 400 h.

CRediT authorship contribution statement

Chieh-Ming Tsai: Writing – original draft, Formal analysis, Data curation, Conceptualization. **Chia-Feng Li:** Validation. **Yu-Ching Huang:** Resources. **Feng-Yu Tsai:** Supervision. **Wei-Fang Su:** Writing – review & editing, Supervision, Project administration.

Declaration of competing interest

The authors declare the following financial interests/personal relationships which may be considered as potential competing interests: Wei-Fang Su reports financial support was provided by National Science and Council of Taiwan. If there are other authors, they declare that they have no known competing financial interests or personal relationships that could have appeared to influence the work reported in this paper.

Acknowledgement

Financial support obtained from National Science and Technology Council of Taiwan (NSTC 111-2923-E-002-012-MY3) for this research is highly appreciated.

Appendix A. Supplementary data

Supplementary data to this article can be found online at https://doi.org/10.1016/j.surfcoat.2024.130695.

References

[1] K.-C. Hsiao, Y.-F. Yu, C.-M. Ho, M.-H. Jao, Y.-H. Chang, S.-H. Chen, Y.-H. Chang, W.-F. Su, K.-M. Lee, M.-C. Wu, Chem. Eng. J. 451 (2023) 138807.
[2] K.-C. Hsiao, M.-H. Jao, K.-Y. Tain, T.-H. Lin, D.-P. Tran, H.-C. Liao, C.-H. Hou, J.-J. Shyue, M.-C. Wu, W.-F. Su, Sol. RRL 4 (2020) 202000197.
[3] M. Mohammadi, S. Gholipour, M.M. Byranvand, Y. Abdi, N. Taghavinia, M. Saliba, ACS Appl. Mater. Interfaces 13 (2021) 45455–45464.
[4] P. Holzhey, M. Saliba, J. Mater. Chem. A 6 (2018) 21794.
[5] P.-H. Lee, T.-T. Wu, C.-F. Li, D. Glowienka, Y.-X. Huang, S.-H. Huang, Y.-C. Huang, W.-F. Su, Sol. RRL 6 (2022) 2100891.
[6] F. Bella, G. Griffini, J.-P. Correa-Baena, G. Saracco, M. Grätzel, A. Hagfeldt, S. Turri, C. Gerbaldi, Science 354 (2016) 203–206.
[7] L. Xiang, F.L. Gao, Y.X. Cao, D.Y. Li, Q. Liu, H.L. Liu, S.T. Li, Org. Electron. 106 (2022) 106515.
[8] Y.T. Wang, I. Ahmad, T.L. Leung, J.Y. Lin, W. Chen, F.Z. Liu, A.M.C. Ng, Y. Zhang, A.B. Djurišić, ACS Mater. Au 2 (2022) 215–236.
[9] L. Shi, T.L. Young, J.C. Kim, Y. Sheng, L. Wang, Y.F. Chen, Z.Q. Feng, M.J. Keevers, X.J. Hao, P.J. Verlinden, M.A. Green, A.W.Y. Ho-Baillie, ACS Appl. Mater. Interfaces 9 (2017) 25073–25081.
[10] A. Uddin, M.B. Upama, H.M. Yi, L.P. Duan, Coatings 9 (2019) 65.
[11] D.-Y. Su, Y.-H. Kuo, M.-H. Tseng, Feng-Yu Tsai, J. Coat. Technol. Res. 16 (2019) 1751–1756.
[12] Y.F. Lv, H. Zhang, R. Liu, Y.N. Sun, W. Huang, ACS Appl. Mater. Interfaces 12 (2020) 27277–27285.
[13] F. Bella, G. Leftheriotis, G. Griffini, G. Syrrokostas, S. Turri, M. Grätzel, C. Gerbaldi, Adv. Funct. Mater. 26 (2016) 1127–1137.
[14] M. Wong-Stringer, O.S. Game, J.A. Smith, T.J. Routledge, B.A. Alqurashy, B. G. Freestone, A.J. Parnell, N. Vaenas, V. Kumar, M.O.A. Alawad, A. Iraqi, C. Rodenburg, D.G. Lidzey, Adv. Energy Mater. 8 (2018) 1801234.
[15] C.A. Aranda, L. Caliò, M. Salado, Crystals 11 (2021) 519.
[16] S.J. Kim, T.Y. Kim, B.H. Kang, G.-H. Lee, B.-K. Ju, RSC Adv. 8 (2018) 39083.
[17] E. Ramasamy, V. Karthikeyan, K. Rameshkumar, G. Veerappan, Mater. Lett. 250 (2019) 51–54.

[18] R.D. Maksimov, S. Gaidukov, J. Zicans, J. Jansons, Mech. Compos. Mater. 44 (2008) 505–514.
[19] C.-C. Lin, S.-H. Hsu, Y.-L. Chang, W.-F. Su, J. Mater. Chem. 20 (2010) 3084–3091.
[20] J.H. Park, S.-D. Baek, J.I. Cho, J.Y. Yoo, S.-Y. Yoon, S.H. Kim, S.Y. Lee, Y.S. Kim, J.-M. Myoung, Compos. B Eng. 175 (2019) 107188.
[21] C. Wolf, H. Angellier-Coussy, N. Gontard, F. Doghieri, V. Guillard, J. Membr. Sci. 556 (2018) 393–418.
[22] P.E. Keller, R.T. Kouzes, Water Vapor Permeation in Plastics, Richland, Washington, Pacific Northwest National Laboratory, 2017, p. 26070.
[23] W.F. Su, Principles of Polymer Design and Synthesis, Chapter 4, Springer, Heidelberg, Germany, 2013.
[24] C.Y. Chang, Y.C. Huang, C.S. Tsao, W.F. Su, ACS Appl. Mater. Interfaces 8 (2016) 26712–26721.